ACS APPLIED MATERIALS & INTERFACES

www.acsami.org

Research Article

Bioinspired Manufacturing of Aerogels with Precisely Manipulated Surface Microstructure through Controlled Local Temperature Gradients

Halil Tetik, Dan Feng, Samuel W. Oxandale, Guang Yang, Keren Zhao, Katelyn Feist, Nasrullah Shah, Yiliang Liao, Zayd C. Leseman, and Dong Lin*

Cite This: *ACS Appl. Mater. Interfaces* 2021, 13, 924–931

Read Online

ACCESS | Metrics & More | Article Recommendations

ABSTRACT: The freeze casting process has been widely used for fabricating aerogels due to its versatile and environmentally friendly nature. This process offers a variety of tools to tailor the entire micropore morphology of the final product in a monolithic fashion through manipulation of the freezing kinetics and precursor suspension chemistry. However, aerogels with nonmonolithic micropore morphologies, having pores of various sizes located in certain regions of the aerogels, are highly desired by certain applications such as controlled drug-delivery, bone tissue engineering, extracellular simulation, selective liquid sorption, immobilized catalysts, and separators. Furthermore, aerogels composed of micropores with predesigned size, shape, and location can open up a new paradigm in aerogel design and lead to new applications. In this study, a general manufacturing approach is developed to control the size, shape, and location of the pores on the aerogel surface by applying a precise control on the local thermal conductivity of the substrate used in a unidirectional freeze casting process. With our method, we created patterned low and high thermal conductivity regions on the substrate by depositing patterned photoresist polymer features. The photoresist polymer has a much lower thermal conductivity, which resulted in lower cooling/freezing rates compared to the silicon substrate. Patterned thermal conductivity created a designed temperature profile yielding to local regions with faster and slower freezing rates. Essentially, we fabricated aerogels whose micropore morphology on their surface was a replica of the patterned substrates in terms of size and location of the micropores. Using the same substrates, we further showed the possibility of 3D printed aerogels with precisely controlled, surface micropore morphologies. To the best of our knowledge, this is the first study that reports aerogels having micropore morphologies (e.g., size, shape, and location) that are precisely controlled through locally controlled thermal conductivity of the substrates.

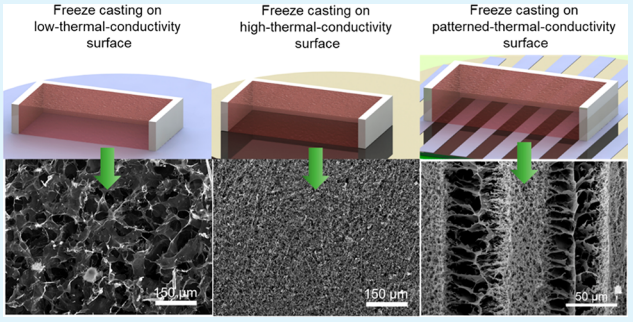

KEYWORDS: *aerogel, micropore, freeze casting, microstructure manipulation, controlled local thermal conductivity, 3D printing*

1. INTRODUCTION

Aerogels are highly porous materials whose porosity is achieved by replacing the liquid component of a wet gel with air.[1] Material properties of aerogels are directly affected by their micropore structures and use of a specific aerogel for a particular application requires precise control of its microporosity.[2] For instance, the micropore structure of the aerogels can be tailored for best mechanical properties,[3] piezoresistivity,[4] thermal conductivity,[5] absorption performance,[6] optical transmittance,[7,8] electromagnetic interference shielding efficiency,[9] etc. Freeze casting, which is a widely utilized method for fabrication of aerogels and porous structures from a variety of materials, offers many different tools for tailoring the microstructure of the final product. Freeze casting parameters used for manipulating the microstructure of the final product have been deeply investigated and several review papers have been published.[10−13] Typically, freeze casting produces a homogeneous micropore morphology where micropore size is controlled through tuning the freeze casting parameters. However, applications like bone tissue engineering, controlled multidrug delivery, selective liquid absorption, and separating membranes may benefit from nonhomogeneous micropore morphologies, that is, having pores of varying sizes,

Received: October 29, 2020
Accepted: December 28, 2020
Published: January 5, 2021

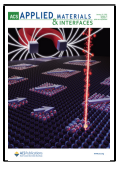

https://dx.doi.org/10.1021/acsami.0c19087
ACS Appl. Mater. Interfaces 2021, 13, 924–931

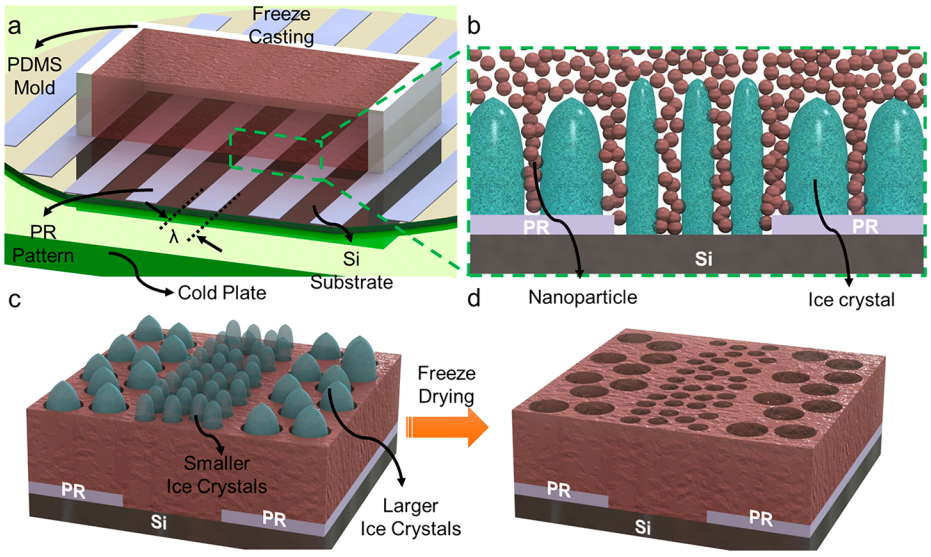

Figure 1. Schematics of proposed process: (a) Si substrate with PR patterns placed on top of a cold plate. Aqueous suspension is poured into a PDMS mold placed on top of the Si substrate for freeze casting. (b) Before freezing, the aqueous suspension is composed of water and homogeneously dispersed nanoparticles. (c) Once the temperature of the cold plate is reduced, the freezing process is initiated on the top of the PR and Si surfaces. Due to the difference in thermal conductivity of both surfaces, the average size of the ice crystals varies. (d) After freeze-drying sublimates all the ice content, the porosity is obtained as a replica of the patterned PR features.

those are located in specific, controlled regions of the aerogels. Fabricating aerogels with a controlled nonhomogeneous microstructure has always been a challenge. Furthermore, in the age of atomic and close to atomic scale manufacturing,[14,15] controlling the pore morphology of the aerogels with a micrometer resolution would be of the interest.

To address this issue, several researchers performed sequential freeze casting of multiple slurries to mimic the bone microstructure.[16,17] Since the increasing solid content of the slurry yields to pores with decreasing size, they performed a two-step freeze casting procedure using slurries with low and high solid loadings. Using this method, they achieved bone-like scaffolds with larger pores at the center surrounded by much smaller pores at the shell. Ogden et al. on the other hand, used an ultrasound-directed self-assembly method to achieve a control on the microstructure during the freeze casting process.[18] They used an ultrasound wave field to drive the nanoparticles in the slurry into a concentric ring pattern achieving alternating regions with low and high porosities. In another study, Yang et al. reported that surface wettability of the substrate used for freeze casting has a significant effect on micropore size.[19] They showed that performing freeze casting on a hydrophilic substrate leads to small pores, whereas a hydrophobic substrate results in large pores. They fabricated substrates with various wetting behaviors and were able to manipulate the microstructure of the freeze-casted aerogels. Even though these studies achieved nonmonolithic microstructures with controlled size and location of the micropores, proposed processes are complex, and lack design possibilities, high resolution, and clear boundaries between different pore-size regions.

Thermal conductivity of the substrates used in a unidirectional freeze casting process has a significant impact on the nucleation and growth of ice crystals during the freezing as well as the micropore morphology of the final product.[20] Herein, we benefited from this phenomenon and fabricated substrates with varying thermal conductivity patterns, which was achieved by fabricating patterned photoresist (PR) polymer features on a silicon (Si) wafer following a lithography process. The difference in thermal conductivity between PR and Si yielded to nonmonolithic microstructures on the surface of the aerogels with micropores whose size and location can be controlled by the user. We selected two common freeze-cast suspensions such as colloidal silica and graphene oxide (GO) as base materials to demonstrate our method as a general approach. Furthermore, by adjusting the temperature of the cold plate used in the freeze casting procedure, the average size of the pores at different regions can be tailored for different size requirements. Using the Si substrates with patterned PR features, we distinguished boundaries between the regions with small and large pores and achieved a resolution as low as ~50 μm. We further showed the possibility of 3D-printed aerogels with precisely controlled surface micropore morphologies. To the best of our knowledge, this is the first study to report aerogels with controlled micropore morphologies (e.g., pore size, shape, and location) precisely controlled by creating thermal conductivity patterns on the substrates. We believe our method can be further extended for controlling pore size and location in 3D, and can be beneficial for applications such as drug delivery, bone tissue engineering, photo catalysis, pollutant absorption from water, etc.

2. RESULTS AND DISCUSSION

In the freeze casting method, thermal conductivity of the substrate has a tremendous effect on the cooling rate of the slurry, nucleation and growth of the ice crystals, and eventually the final microstructure.[20] To date, in all reported cases, substrates with uniform thermal conductivities were used. Here in this work, we prepared Si wafer substrates with patterned PR features that are deposited by photolithography. Using these substrates with patterned PR features, we performed unidirectional freeze casting procedures as schematically described in Figure 1a. Patterned PR features on the Si substrate were parallel stripes with a feature size (width) of λ. To test the effect of different stripe dimensions, we fabricated patterned PR features with varying λ values on Si substrates. The

https://dx.doi.org/10.1021/acsami.0c19087
ACS Appl. Mater. Interfaces 2021, 13, 924−931

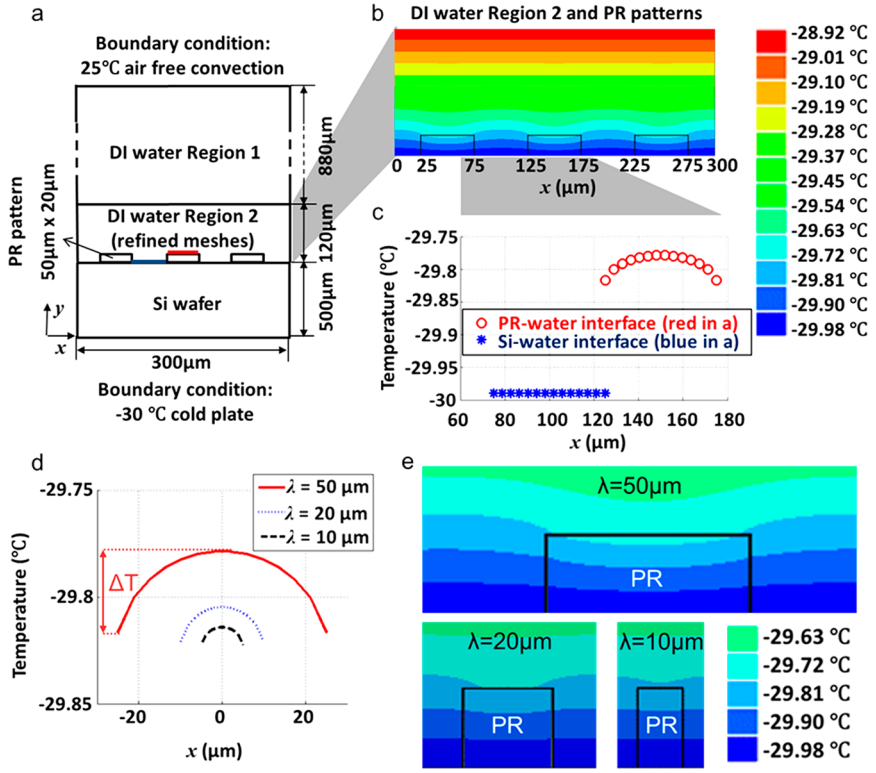

Figure 2. (a) The sketch, dimensions, and boundary conditions of a 2D model for FEA simulation. (b) The 2D temperature profile in the neighborhood of Si, PR, and DI interfaces. (c) The temperature curves of PR−water interface and Si−water interface. (d) Temperature curves of PR−water interface with various λ values. (e) 2D temperature profiles in the neighborhood of PR patterns with varying λ values.

relatively low thermal conductivity ($0.19 W\cdot(m\cdot K)^{-1}$)[21] of the PR features compared to Si ($149 W\cdot(m\cdot K)^{-1}$)) helped us to manipulate the temperature gradient above the PR and Si surfaces. To achieve a unidirectional freeze casting process, we poured the prepared aqueous suspensions into a PDMS wall structure, which was placed on top of the PR-featured Si substrate. At this stage, the poured suspension contained liquid water and homogeneously dispersed nanoparticles. Thereafter, the substrate was placed on top of a precooled cold plate, whose temperature was well below the freezing point of water and was used to manipulate the rate of freezing. Due to the difference in the thermal conductivities of those surfaces, nucleation and growth rate of the ice crystals differed and resulted in a variation in the ice crystal size. As schematically demonstrated in Figure 1b,c, due to a higher thermal conductivity of the Si substrate surface, we obtained fine-sized ice crystals. The size was much coarser on the PR feature surface where the thermal conductivity was much lower. Once the frozen structures were freeze-dried, we obtained a surface porosity that replicates the patterned PR features on the Si substrate (Figure 1d). Even though we only generated patterned PR features as parallel stripes to find the minimum resolution, it is also possible to deposit the PR polymer in a designed 2D shape, which will result in a micropore structure in a desired pattern.

To better illustrate how the unidirectional freeze casting using Si substrates with patterned PR features works, we used finite-element analysis (FEA) and simulated the temperature field around the aqueous suspension−Si wafer interface and the aqueous suspension−PR patterns interface. We used several assumptions for simplifying the model as explained in the experimental section. The geometry that covered three PR stripes as shown in Figure 2a was constructed to represent the repeated stripes in our simulations. We ignored the effect of the PDMS mold, since the size is much larger than the PR stripes and the aqueous suspension was represented as pure DI water because the concentration of slurries used was low (less than 1 wt % for GO). Since there is no body-heat flux on the model domain, the heat equation for the 2D model given in Figure 2a can be written as

$$k(T(x, y)_{,xx} + T(x, y)_{,yy}) = 0 \quad (1)$$

where k is the heat conductivity, x and y are spatial coordinates, "," indicates a spatial derivative, and T is the temperature. Equation 1 can be rewritten to a weak form as

$$\int_0^X \int_0^Y (k\delta T_{,x} T_{,x} + k\delta T_{,y} T_{,y})\mathrm{d}y\mathrm{d}x = \int_0^Y k\delta T T_{,x}\mathrm{d}y|_{x=0}^{x=X} + \int_0^X k\delta T T_{,y}\mathrm{d}x|_{y=0}^{y=Y} \quad (2)$$

After our simulations, we obtained the temperature profile in the neighborhood of Si, PR, and DI interfaces as presented in Figure 2b. As clearly seen there, we obtained a wavy temperature profile on the heights that is close to the substrate and patterned PR features. As the height is increasing, the temperature profile becomes more uniform. Due to the temperature profile reaching to equilibrium and becoming uniform after a certain height above the substrate, we only observed the patterned microstructure on the surface of the aerogels. However, we believe that by performing an optimization study for parameters such as the thermal conductivity values of the materials used, dimension of the patterns, and initial temperatures, we think the wavy temperature profile can be extended much above the substrate

https://dx.doi.org/10.1021/acsami.0c19087
ACS Appl. Mater. Interfaces 2021, 13, 924−931

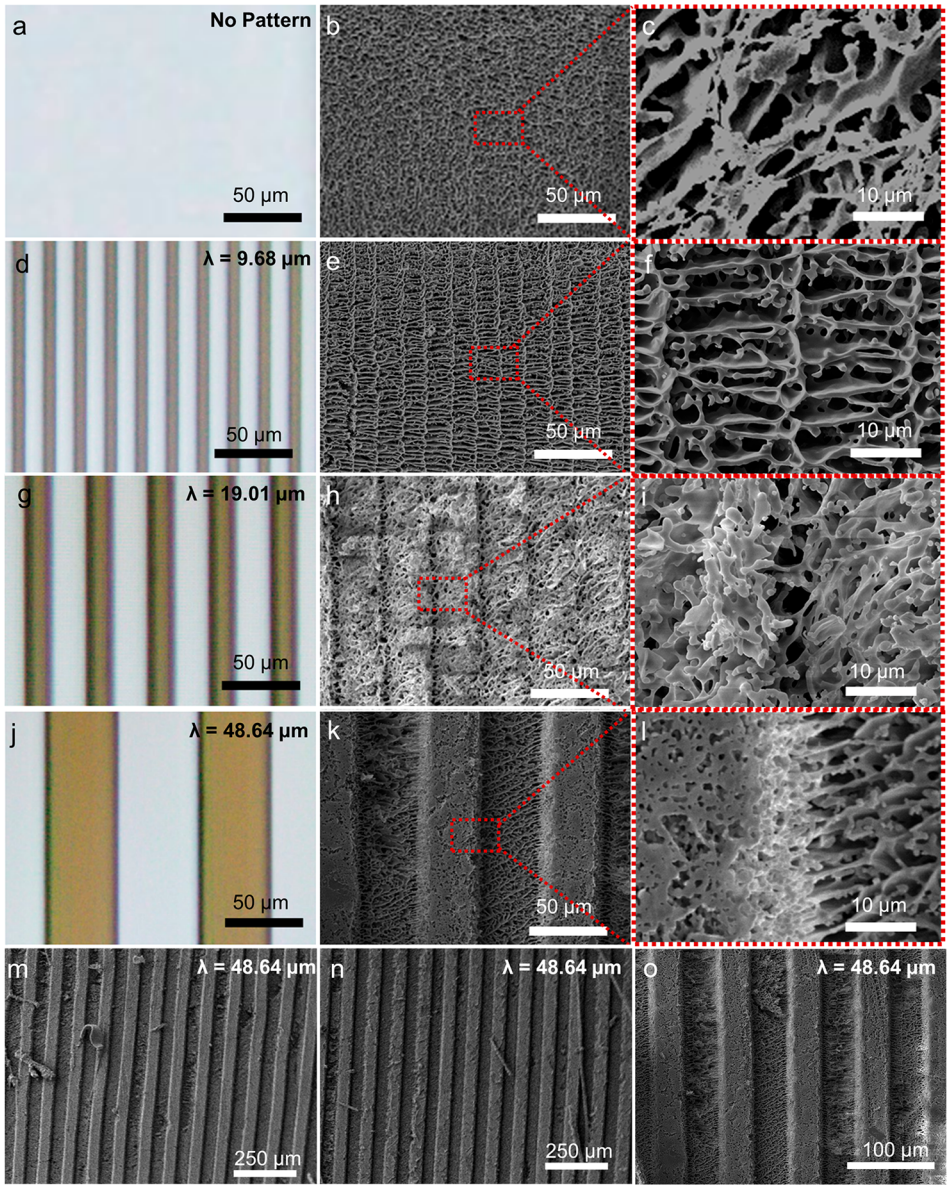

Figure 3. Optical microscope images showing the Si substrates with PR patterns and SEM images showing the effect of the PR pattern feature size on the microstructure of the freeze-casted silica; (a–c) without PR pattern, (d–f) λ = 9.68 μm, (g–i) λ = 19.01 μm, and (j–o) λ = 48.64 μm.

surface and can be used to tune the microstructure of the aerogels in 3D. To compare the temperature curves of PR–water and Si–water interfaces, we prepared the 2D temperature profile given in Figure 2c. Due to a lower thermal conductivity, the temperature of water at the PR–water interface is higher than that of the water at the same height above bare silicon. Therefore, the water above the PR freezes more slowly than the water at the same height above the Si surface and the water in contact with the Si wafer to freeze earlier and grow smaller ice crystals than water contacting PR patterns. As the above-mentioned simulations were performed for a feature size of λ = 50 μm, we also provided the simulation results for much smaller feature size values (λ = 20, and 10 μm) to see the effect of the feature size on the temperature profile above the patterned substrate. As given in Figure 2d, with the decreasing λ values, the difference between the maximum and minimum temperature at the PR–water interface (ΔT) reduces. Furthermore, as presented in Figure 2e, wavy temperature profile in the vicinity of PR–water interface, which is the driving force for making distinct region of the different pore size, becomes flatter across the surface of the substrate. This change in the temperature profile obtained with the decreasing λ would make it harder to obtain a patterned microstructure as confirmed by the SEM images given in Figure 3 for λ = 9.68 and 19.01 μm cases.

We first investigated the fabricated Si substrates with and without PR patterned features, as presented in Figure 3a,d,g, using an optical microscope. Widths of the PR pattern features (λ) were measured as 48.64, 19.01, and 9.68 μm for a designed λ of 50, 20, and 10 μm, respectively, while the width of the gaps between PR stripes were measured as 52.24, 21.87, and 10.55 μm. For each λ value, a distinct boundary between the PR features and the Si surface was obtained and the height of each pattern was measured as approximately 20 μm. To understand how these features affect the microstructure of the fabricated aerogels, we freeze-casted colloidal silica suspension and investigated their microstructure as presented in Figure 3. In Figure 3b,c, we provided the control experiment where

https://dx.doi.org/10.1021/acsami.0c19087
ACS Appl. Mater. Interfaces 2021, 13, 924–931

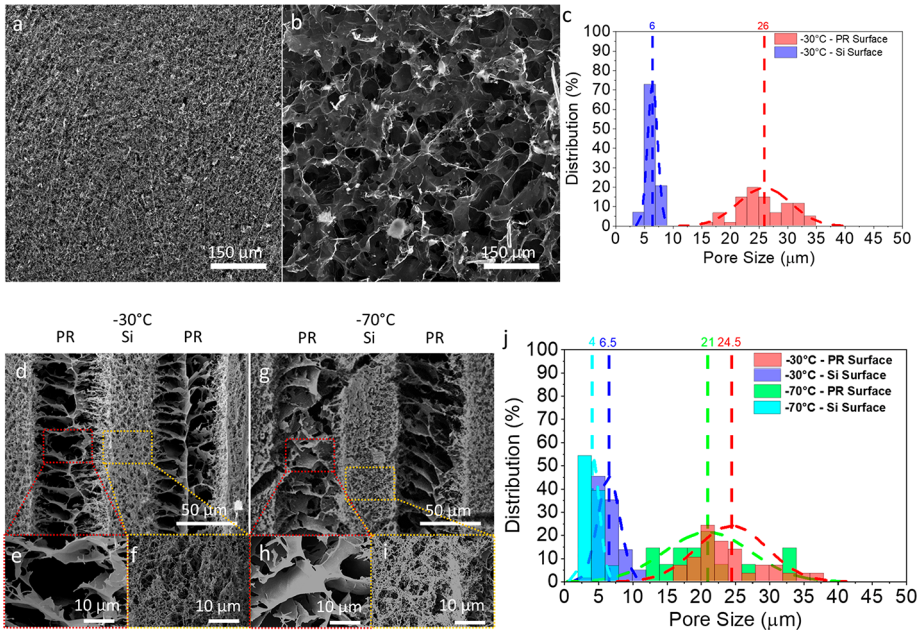

Figure 4. (a) SEM image of the GO aerogel freeze casted on Si substrate with a cold plate temperature of −30 °C. (b) SEM image of the GO aerogel freeze casted on Si substrate covered with PR layer without any pattern with a cold plate temperature of −30 °C. (c) Size distribution of the pores on the aerogel surfaces given in a and b. (d−f) SEM images of the GO aerogel freeze casted on Si substrate patterned with PR features (λ = 48.64 μm) with a cold plate temperature of −30 °C. (g−i) SEM images of the GO aerogel freeze casted on Si substrate patterned with PR features (λ = 48.64 μm) with a cold plate temperature of −70 °C. (j) Average size distribution of the pores on the aerogel surfaces given in d and g.

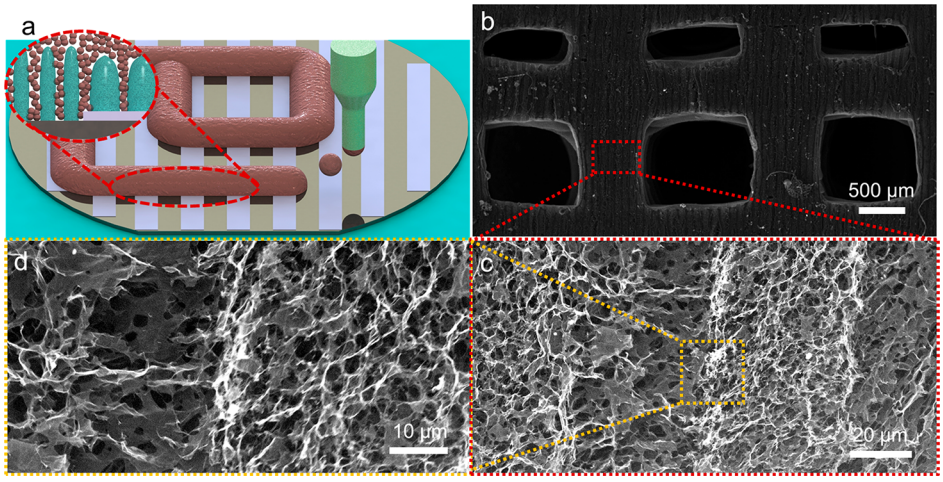

Figure 5. (a) Schematics of the 3D freeze printing process using substrates with patterned PR features. (b−d) Low and high-magnification SEM images showing the tailored microstructure of the graphene oxide aerogels fabricated through the 3D freeze printing process using the patterned Si substrate with λ = 48.64 μm.

there was no PR feature on the Si substrate. As seen in the scanning electron microscope (SEM) images, the microstructure morphology was identical to common unidirectional freeze casting. When λ = 9.68 μm, we observed that patterned PR features had affected the freeze casting process and resulted in a patterned orientation in the pore morphology (Figure 3e,f). However, we did not observe any trace on controlled location of varying pore size. Even though the substrate having patterned PR features with λ = 19.01 μm showed some traces of location control on the pore size, the distinction between different-sized regions was not clear. Also, the width (λ) of the regions with different pore sizes did not match with the patterned PR features (Figure 3h,i). With λ = 48.64 μm, we obtained a spatial control on the micropore-sized distribution as a replica of the patterned PR features on the Si substrate (Figure 3k,l). The border between regions with different pore size was distinct, as it can be seen from the high-magnification SEM image given in Figure 3l. We further provided low-magnification SEM images of the λ = 48.64 μm case to show the long-range control on the microstructure of the aerogel surfaces in Figure 3m,o.

To demonstrate it as a general method, we also freeze-casted a GO suspension since reduced graphene oxide is one of the most common functional aerogels fabricated by freeze casting. We first fabricated two control specimens, using a Si substrate without any PR features and Si substrates covered with PR (without patterning) using a cold plate temperature of −30 °C. As presented in Figure 4a,b, the average pore size of the sample

https://dx.doi.org/10.1021/acsami.0c19087
ACS Appl. Mater. Interfaces 2021, 13, 924−931

fabricated on top of the Si substrate without PR is much finer when compared to the sample fabricated on top of the Si substrate with PR. The average pore size was measured as ∼26 and 6 μm with and without PR cases, respectively (Figure 4c). In our experiments with the substrates having patterned features (λ = 48.64 μm), we used two different (−30 °C and −70 °C) cold plate temperatures to investigate the effect of the freeze temperature on the microstructure. With a cold surface temperature of −30 °C, we have obtained a microporosity as a replica of the patterned PR features as presented in Figure 4d. The high magnification SEM images clearly show the difference between the average size of the pores on PR (Figure 4e) and Si (Figure 4f) surfaces. When we reduced the cold plate temperature to −70 °C and repeated the freeze casting procedure using the same GO suspension, we obtained the microstructure provided in Figure 4g. The distinction between the regions having different pore-size distribution is as clear as the other cases at −30 °C cold plate temperature. Average pore size on the other hand is much smaller in both regions due to the much faster freezing rate. To quantify the difference between −30 °C and −70 °C cold plate temperature cases, we have used an image-processing software (ImageJ) to help us measure the average size of individual pores. As given in Figure 4j, the average size of the pores increased from ∼6.5 μm to ∼24.5 μm when the substrate surface changed from Si to PR for the cold plate temperature of −30 °C. With the lower cold plate temperature (−70 °C), average size of the pores for both surfaces was much finer compared to the −30 °C plate due to a much faster freezing rate.[10−12] While the Si surface yielded to an average pore size of ∼4 μm, the PR surface resulted in ∼21 μm. Measured pore size for the −30 °C case was also in a good agreement with results provided in Figure 4c.

In order to eliminate the dependency of freeze casting method on molds, our group recently developed a 3D freeze printing (3DFP) method, which is a hybrid method composed of unidirectional freeze casting and drop-on-demand (DOD) printing.[22−25] In a 3DFP process, droplets of liquid precursors are generated using a DOD dispenser and are deposited on top of a substrate whose temperature is well below the freezing point of the solvent used in the liquid precursor (Figure 5a). As droplets reach the precooled substrate, the solvents experience an immediate freezing, which allows them to preserve their shape. With the reduced distance and time between separate droplets, uniform lines can be obtained after the coalescence.[26] Using these lines, complex 3D frozen structures can be achieved by a mold-free method. Frozen structures with desired shapes are freeze-dried, which sublimates the solvent crystals and a porous aerogel is obtained. Since 3DFP involves freeze casting, the microstructure of the final aerogel can be manipulated by the freezing kinetics. To further increase the impact of the proposed freeze casting method by increasing the freedom in material design, we investigated the effect of the patterned PR features on the microstructure of 3D freeze printed GO aerogels. For this experiment, we used a 5 mg·mL^{-1} GO suspension along with PR-patterned Si substrates (λ = 48.64 μm) and fabricated scaffolds as presented in Figure 5b. With the high-magnification SEM images presented in Figure 5c,d, we observed the microstructure of the 3D freeze printed aerogels is also manipulated with the patterned PR features on the Si substrate. As we observed in the previous cases (unidirectional freeze casting using silica and GO-based suspensions), we have seen that due to thermal conductivity on the patterned PR features, the pore size (∼15 μm) is much larger than the regions without patterned PR features (∼5 μm).

3. CONCLUSIONS

In summary, we used substrates with patterned thermal conductivities to fabricate aerogels with designed surface porosities in terms of size and location of the micropores. The patterned thermal conductivity was obtained as a replica of PR features on the Si substrates deposited by a lithography process. Due to patterned thermal conductivity of the substrates, we obtained a wavy temperature profile above the surface, which manipulated the nucleation and growth of the ice crystals during the freeze casting process. On the surface of the final aerogels, we observed larger ice crystals above the PR surface, while the ice crystals were much smaller above the Si surface. The aerogels fabricated through our method exhibited a designed surface micropore morphology, in which size and location of the pores can be determined by the user. Our experiments with the 3D freeze printing method also showed that substrates with varying thermal conductivities can be further implemented to a 3D printing processes based on a freeze casting method to fabricate aerogels with custom macro and microstructures. We think that by further improving/optimizing thermal conductivity patterns on the substrates, the control on the microstructure morphology on the aerogel surface can be extended to 3D.

4. MATERIALS AND METHODS

4.1. Preparation of the PR Patterns on Si Wafer Substrates. For the substrates, we used 4-in.-diameter silicon wafers. To begin the process, AZ 4620 PR was spun onto the Si wafer, which was then soft-baked on a 110 °C hot plate for 80 s with full contact. A second layer of AZ 4620 PR was then spun onto the wafer, followed by a 180 s soft-bake on a 115 °C hot plate with full contact. The final thickness of the PR was approximately 24 μm. After applying the PR, it was patterned using photolithography. Using a patterned photomask, the wafer was exposed to a dose of 1742 mJ·cm^{-2}. The pattern was then developed through submersion in AZ 400 K 1:4 for 300 s. The wafer was then placed in an oven at 200 °C to hard-bake the PR pattern. After fabrication, resulting heights of the PR features were measured and found to be in the range of 15−19 μm.

4.2. Freeze Casting Procedure. For the freeze casting process, we used a commercially available colloidal silica suspension (Nyacol, DP9711) with a concentration of 30 wt % and an average particle size of 20 nm. We prepared the GO suspension by adding graphene oxide powder (Cheaptubes Inc.) into DI water and using sonication for 30 min. The concentration of the GO suspension was set to 8 mg·mL^{-1}. To obtain aerogels with spatially controlled porosity, we prepared the freeze casting setup described in Figure 1a. First, we prepared square polydimethylsiloxane (PDMS) (Dow Corning, Sylgard 184) walls to be used as bottomless molds for the freeze casting process according to the manufacturer's directions. Briefly, we first prepared 3D printed polylactic acid (PLA) molds using a commercially available fused deposition modeling type 3D printer to shape the PDMS molds. Then, we mixed the PDMS with curing agents of 10:1 weight ratio. The mixture was kept in a vacuum chamber for 30 min to remove gas bubbles. Finally, the mixture was poured inside the already prepared 3D printed PLA molds and cured for 24 h in ambient temperatures. To freeze-cast the suspensions, we poured the prepared suspension inside the PDMS wall structure placed on the PR-patterned Si wafer substrate, which was placed on top of a precooled cold plate (Instec, HCP204SG). We pushed the PDMS wall firmly from the top to ensure there was no leakage after pouring the suspensions. We left the suspensions at the target temperature for at least 30 min to ensure

https://dx.doi.org/10.1021/acsami.0c19087
ACS Appl. Mater. Interfaces 2021, 13, 924−931

complete freezing. Frozen samples were moved to a −70 °C freezer for further crystallization and then a subsequent freeze-drying was applied at −35 °C and 0.02 mbar using a commercial freeze-dryer (Labconco, Freezone Triad).

4.3. FEA Simulations. We simplified the model with several assumptions. First, all materials were assumed to be homogeneous and isotropic, with thermal properties independent of temperature change. The PR stripes were assumed to have consistent width and gap distance so the temperature distribution was uniform along the PR stripe direction. We simplified the model with the region covering three PR stripes as shown in Figure 2 to represent the repeated stripes. We ignored the effect of PDMS mold, since the size is much larger than the PR stripes. The aqueous slurry was represented as pure DI water since the concentration was very low. Because we were more interested in the temperature profile discrepancy between aqueous suspension−Si wafer interface and the aqueous suspension−PR patterns interface, rather than the exact transient temperature during the process, the simulation was at steady state. In addition, the initial temperature of water affected the freezing rate (i.e., Mpemba effect), the reason for which is still unclear. We ignored the phase change of DI water, because a phase-change problem requires an FEA solver with transient analysis or quasi-static iterations to update the physical properties. As discussed in previous assumptions, we were more interested in the trend of temperature-profile discrepancy between the two interfaces. The model was built in ABAQUS, following the sketch and dimensions as shown in Figure 2a. There were six parts in the model, including three PR patterns, Si wafer, a DI water region with refined meshes, and a DI water region with coarse meshes. Boundary conditions were chosen to satisfy right-hand side of eq 2:

1. There was no heat flux on $x = 0,X$ (i.e., Neumann boundary conditions $T(x = 0.y)_{,x} = 0$, $T(x = X.y)_{,x} = 0)$).
2. The precooled cold plate offered a Dirichlet boundary condition to the bottom of the Si wafer with a constant temperature of −30 °C (i.e., $T(x,y = 0) = -30$ °C).
3. The air on top of DI water provides a Neumann boundary condition by free convection with a 25 °C room temperature and a film coefficient of 5 $W\cdot(m^2\cdot K)^{-1}$ (i.e., $T(x,y = Y)_{,y} = h(T(x,y = Y) - T_{air})$, where h is the film coefficient and T_{air} is the room temperature).

We chose DC2D4 (a four-node, linear heat-transfer quadrilateral) element for all the parts. Since the simulation was at steady state, we only needed the heat conductivity of each material, which were 0.19 $W\cdot(m\cdot K)^{-1}$, 149 $W\cdot(m\cdot K)^{-1}$, and 0.58 $W\cdot(m\cdot K)^{-1}$ for PR, Si, and DI water, respectively. After our convergence study, we chose to use 65 elements for each PR pattern, 9,375 elements for Si wafer, 2,115 elements for the DI water region with refined meshes, and 3,290 elements for the DI water region with coarse meshes.

4.4. 3D Freeze Printing Procedure. We used a similar inkjet-based 3D printing method that had been reported in other studies.[26] Briefly, as a prepared GO suspension (5 $mg\cdot mL^{-1}$) was loaded inside a syringe barrel attached to a three-axis motion stage. A solenoid microdispensing device was used to generate droplets of GO suspension. Generated droplets were deposited on top of the precooled substrate. By controlling the interdroplet distance and time lapse between droplets with the help of a three-axis motion stage, we 3D printed lines and complex structures after the coalescence of the droplets. Printed structures were freeze-dried using conditions provided for the freeze casting case.

4.5. Surface Characterization of the Fabricated Aerogels. Dried aerogels were investigated under SEM (FEI Versa3D Dual Beam) after sputter-coating the samples with a thin layer of gold (~10 nm). Obtained SEM images were used to investigate characteristics of the micropore morphology of the aerogels. To measure average pore-size distribution, we used an image-processing software (ImageJ).

AUTHOR INFORMATION

Corresponding Author

Dong Lin − *Department of Industrial and Manufacturing Systems Engineering, Kansas State University, Manhattan, Kansas 66506, United States;* orcid.org/0000-0002-1967-2822; Email: dongl@ksu.edu

Authors

Halil Tetik − *Department of Industrial and Manufacturing Systems Engineering, Kansas State University, Manhattan, Kansas 66506, United States;* orcid.org/0000-0003-3647-3822

Dan Feng − *School of Mechanical Engineering, Purdue University, West Lafayette, Indiana 47907, United States*

Samuel W. Oxandale − *Department of Mechanical and Nuclear Engineering, Kansas State University, Manhattan, Kansas 66506, United States*

Guang Yang − *Department of Industrial and Manufacturing Systems Engineering, Kansas State University, Manhattan, Kansas 66506, United States*

Keren Zhao − *Department of Industrial and Manufacturing Systems Engineering, Kansas State University, Manhattan, Kansas 66506, United States*

Katelyn Feist − *Department of Industrial and Manufacturing Systems Engineering, Kansas State University, Manhattan, Kansas 66506, United States*

Nasrullah Shah − *Department of Industrial and Manufacturing Systems Engineering, Kansas State University, Manhattan, Kansas 66506, United States; Department of Chemistry, Abdul Wali Khan University Mardan, Mardan, Khyber Pakhtunkhwa 23200, Pakistan*

Yiliang Liao − *Department of Industrial and Manufacturing Systems Engineering, Iowa State University, Ames, Iowa 50011, United States*

Zayd C. Leseman − *Department of Mechanical and Nuclear Engineering, Kansas State University, Manhattan, Kansas 66506, United States; Department of Mechanical Engineering, King Fahd University of Petroleum & Minerals, Dhahran, Eastern Province 31261, Saudi Arabia*

Complete contact information is available at: https://pubs.acs.org/10.1021/acsami.0c19087

Author Contributions

The manuscript was written through contributions of all authors. All authors have given approval to the final version of the manuscript

Notes

The authors declare no competing financial interest.

ACKNOWLEDGMENTS

D.L. thanks the support of the National Science Foundation under Award No. 1943445 and the support from the Johnson Cancer Center. Z.C.L. acknowledges support from King Fahd University of Petroleum & Minerals' Deanship of Scientific Research under Grant # SR191001. H.T. acknowledges the graduate research scholarship from the Turkish Ministry of National Education.

ABBREVIATIONS

3DFP = 3D freeze printing
DOD = drop-on-demand
FEA = finite-element analysis
GO = graphene oxide
PR = photoresist
PLA = polylactic acid
PDMS = polydimethylsiloxane

https://dx.doi.org/10.1021/acsami.0c19087
ACS Appl. Mater. Interfaces 2021, 13, 924−931

SEM = scanning electron microscope
Si = silicon

REFERENCES

(1) Du, A.; Zhou, B.; Zhang, Z.; Shen, J. A special material or a new state of matter: a review and reconsideration of the aerogel. *Materials* **2013**, *6* (3), 941−968.
(2) Jiménez-Saelices, C.; Seantier, B.; Cathala, B.; Grohens, Y. Effect of freeze-drying parameters on the microstructure and thermal insulating properties of nanofibrillated cellulose aerogels. *J. Sol-Gel Sci. Technol.* **2017**, *84* (3), 475−485.
(3) Yan, L.; Wu, J.; Zhang, L.; Liu, X.; Zhou, K.; Su, B. Pore structures and mechanical properties of porous titanium scaffolds by bidirectional freeze casting. *Mater. Sci. Eng., C* **2017**, *75*, 335−340.
(4) Wu, S.; Ladani, R. B.; Zhang, J.; Ghorbani, K.; Zhang, X.; Mouritz, A. P.; Kinloch, A. J.; Wang, C. H. Strain sensors with adjustable sensitivity by tailoring the microstructure of graphene aerogel/PDMS nanocomposites. *ACS Appl. Mater. Interfaces* **2016**, *8* (37), 24853−24861.
(5) Weigold, L.; Mohite, D. P.; Mahadik-Khanolkar, S.; Leventis, N.; Reichenauer, G. Correlation of microstructure and thermal conductivity in nanoporous solids: the case of polyurea aerogels synthesized from an aliphatic tri-isocyanate and water. *J. Non-Cryst. Solids* **2013**, *368*, 105−111.
(6) Zhu, X.; Yang, C.; Wu, P.; Ma, Z.; Shang, Y.; Bai, G.; Liu, X.; Chang, G.; Li, N.; Dai, J. Precise control of versatile microstructure and properties of graphene aerogel via freezing manipulation. *Nanoscale* **2020**, *12* (8), 4882−4894.
(7) Twej, W. A.; Alattar, A. M.; Drexler, M.; Alamgir, F. M. Tuned optical transmittance in single-step-derived silica aerogels through pH-controlled microstructure. *Int. Nano Lett.* **2017**, *7* (4), 257−265.
(8) Li, T.; Zhou, B.; Du, A.; Xiang, Y.; Wu, S.; Liu, M.; Ding, W.; Shen, J.; Zhang, Z. Microstructure control of the silica aerogels via pinhole drying. *J. Sol-Gel Sci. Technol.* **2017**, *84* (1), 96−103.
(9) Li, C.-B.; Li, Y.-J.; Zhao, Q.; Luo, Y.; Yang, G.-Y.; Hu, Y.; Jiang, J.-J. Electromagnetic Interference Shielding of Graphene Aerogel with Layered Microstructure Fabricated via Mechanical Compression. *ACS Appl. Mater. Interfaces* **2020**, *12* (27), 30686−30694.
(10) Nelson, I.; Naleway, S. E. Intrinsic and extrinsic control of freeze casting. *J. Mater. Res. Technol.* **2019**, *8* (2), 2372−2385.
(11) Li, W.; Lu, K.; Walz, J. Freeze casting of porous materials: review of critical factors in microstructure evolution. *Int. Mater. Rev.* **2012**, *57* (1), 37−60.
(12) Scotti, K. L.; Dunand, D. C. Freeze casting-A review of processing, microstructure and properties via the open data repository, Freeze Casting. *Prog. Mater. Sci.* **2018**, *94*, 243−305.
(13) Liu, R.; Xu, T.; Wang, C.-A. A review of fabrication strategies and applications of porous ceramics prepared by freeze-casting method. *Ceram. Int.* **2016**, *42* (2), 2907−2925.
(14) Fang, F.; Zhang, N.; Guo, D.; Ehmann, K.; Cheung, B.; Liu, K.; Yamamura, K. Towards atomic and close-to-atomic scale manufacturing. *International Journal of Extreme Manufacturing* **2019**, *1* (1), 012001.
(15) Fang, F. Atomic and close-to-atomic scale manufacturing: perspectives and measures. *International Journal of Extreme Manufacturing* **2020**, *2* (3), 030201.
(16) Lee, H.; Jang, T.-S.; Song, J.; Kim, H.-E.; Jung, H.-D. The production of porous hydroxyapatite scaffolds with graded porosity by sequential freeze-casting. *Materials* **2017**, *10* (4), 367.
(17) Tang, Y.; Zhao, K.; Hu, L.; Wu, Z. Two-step freeze casting fabrication of hydroxyapatite porous scaffolds with bionic bone graded structure. *Ceram. Int.* **2013**, *39* (8), 9703−9707.
(18) Ogden, T. A.; Prisbrey, M.; Nelson, I.; Raeymaekers, B.; Naleway, S. E. Ultrasound freeze casting: Fabricating bioinspired porous scaffolds through combining freeze casting and ultrasound directed self-assembly. *Mater. Des.* **2019**, *164*, 107561.
(19) Yang, M.; Wu, J.; Bai, H.; Xie, T.; Zhao, Q.; Wong, T. W. Controlling three-dimensional ice template via two-dimensional surface wetting. *AIChE J.* **2016**, *62* (12), 4186−4192.
(20) Zhao, J.; Li, Y.; Wu, Y.; Lv, S.; Lu, K. Microstructure of TiO2 porous ceramics by freeze casting of nanoparticle suspensions. *Ceram. Int.* **2017**, *43* (17), 14593−14598.
(21) Shokralla, S. A.; Al-Muaikel, N. S. Thermal properties of epoxy (DGEBA)/phenolic resin (NOVOLAC) blends. *Arabian Journal for Science and Engineering* **2010**, *35* (1B), 7−14.
(22) Zhang, Q.; Zhang, F.; Medarametla, S. P.; Li, H.; Zhou, C.; Lin, D. 3D printing of graphene aerogels. *Small* **2016**, *12* (13), 1702−1708.
(23) Yan, P.; Brown, E.; Su, Q.; Li, J.; Wang, J.; Xu, C.; Zhou, C.; Lin, D. 3D printing hierarchical silver nanowire aerogel with highly compressive resilience and tensile elongation through tunable poisson's ratio. *Small* **2017**, *13* (38), 1701756.
(24) Ma, C.; Wang, R.; Tetik, H.; Gao, S.; Wu, M.; Tang, Z.; Lin, D.; Ding, D.; Wu, W. Hybrid nanomanufacturing of mixed-dimensional manganese oxide/graphene aerogel macroporous hierarchy for ultralight efficient supercapacitor electrodes in self-powered ubiquitous nanosystems. *Nano Energy* **2019**, *66*, 104124.
(25) Brown, E.; Yan, P.; Tekik, H.; Elangovan, A.; Wang, J.; Lin, D.; Li, J. 3D printing of hybrid MoS2-graphene aerogels as highly porous electrode materials for sodium ion battery anodes. *Mater. Des.* **2019**, *170*, 107689.
(26) Tetik, H.; Yang, G.; Tan, W.; Fong, A.; Lei, S.; Weker, J. N.; Lin, D. High Speed In-Situ X-Ray Imaging of 3D Freeze Printing of Aerogels. *Additive Manufacturing* **2020**, *36*, 101513.

https://dx.doi.org/10.1021/acsami.0c19087
ACS Appl. Mater. Interfaces 2021, 13, 924−931